Supplementary Material

Insighting the interaction mechanism of zirconium xerogel coagulants and humic acids: the protective effect of acetylacetone

Jun Guo[a], Xia Xu[b*], Shiyao Bu[b], Ruoying Yang[a], Yingang Xue[a], Qiuya Zhang[b], Mingguo Peng[b]

[a] School of Environmental Science and Engineering, Changzhou University, Changzhou, 213164, China

[b] School of Urban Construction, Changzhou University, Changzhou, 213164, China

[*]Corresponding Author: Xia Xu E-mail address: xuxia20041982@163.com

Tel: +86 15061128088

[*]**Corresponding Author.**

E-mail address: xuxia20041982@163.com (Xia Xu)

S1. Details about the properties of simulated water

Table S1. The quality information of simulated water

Name	Turbidity (NTU)	UV_{254} (cm^{-1})	DOC (mg/L)	pH
Kaolin-HA simulated water (10 mg HA/L)	26±0.5	0.256	15.6	6.8
Kaolin-HA simulated water (40 mg HA/L)	46.7±0.5	1.447	36.4	6.4
Kaolin-HA simulated water (80 mg HA/L)	66.3±0.5	2.825	57.4	6.6

S2. Details about the schematic diagram of the combined device

Solution conductivity was often used to measure the concentration of salt ions in aqueous solutions. To further understand the hydrolytic polymerization process of ZXC in solution, the stability of the hydrolytic process of the coagulant was evaluated by alkali-titration combined with electrical conductivity measurement. As shown in the **Figure S2a**, there was no significant difference between $ZrCl_4$ and ZXC coagulants with different AcAc concentrations in the decrease of electrical conductivity. This proves that the introduction of AcAc did not inhibit the interaction between Zr^{4+} and OH^-. However, the introduction of H_2O in the preparation process significantly improved the saturation of ZXC coagulant (**Figure S2b**). The electrical conductivity in coagulant solution was believed to be derived from Zr^{4+} and Cl^-, while the introduction of Na^{2+} and OH^- ions into aqueous solution will form $NaCl_2$ and $Zr(OH)_4$ precipitates. The right shift of saturation point was considered to be the presence of higher amount of Cl ions in unit solution, while the increase of saturation conductivity was considered to be the presence of lower amount of Zr in solution. Therefore, excess H_2O was thought to affect the number of effective Zr^{4+} in the ZXC coagulant.

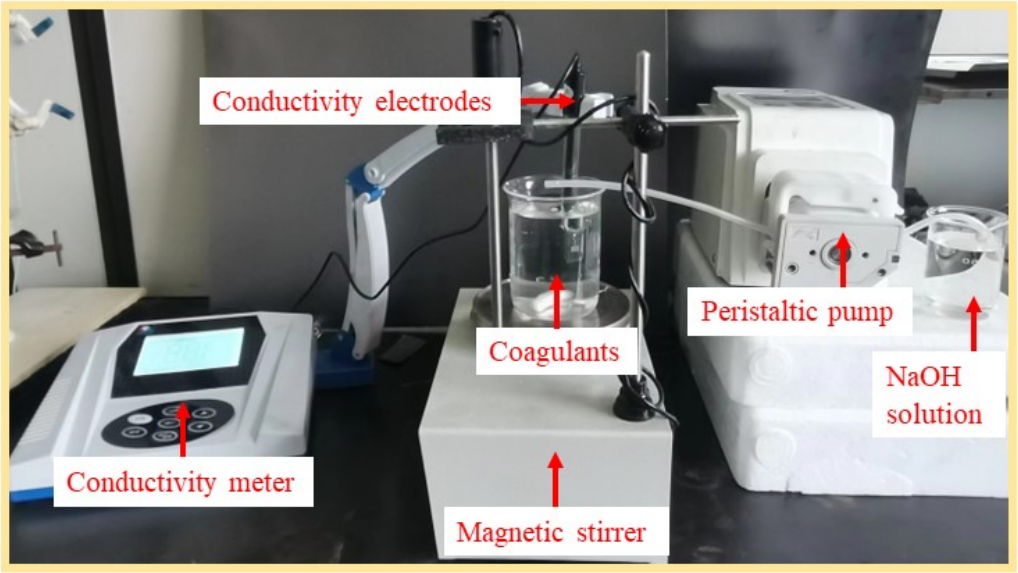

Figure S1. The schematic diagram of the combined device

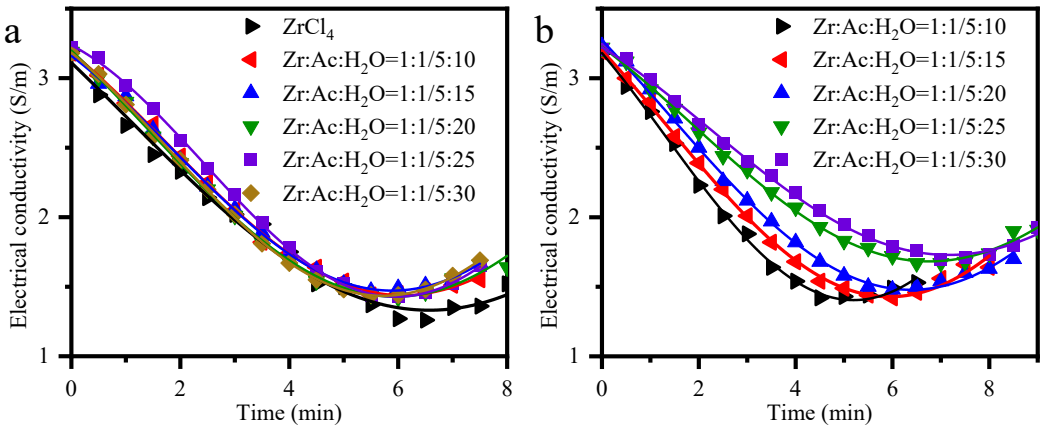

Figure S2. The electrochemical analysis of coagulants in deionized water.

S3 Details about the preparation of PAC

A PAC storage solution (0.1 mol-(Al^{3+})/L) with an OH/Al molar ratio of 1.5 was prepared by a slow alkaline titration method. $AlCl_3 \cdot 6H_2O$ (6.2051 g) powders were dissolved in about 100 mL of deionized water. Na_2CO_3 (2.0431 g) powders were dissolved, and then the Na_2CO_3 solution was slowly added to the $AlCl_3$ solution under stirring. The mixture was stirred for 4 h and then transferred to a 250 mL volumetric flask.

S4 Optimized Preparation Conditions for ZXC

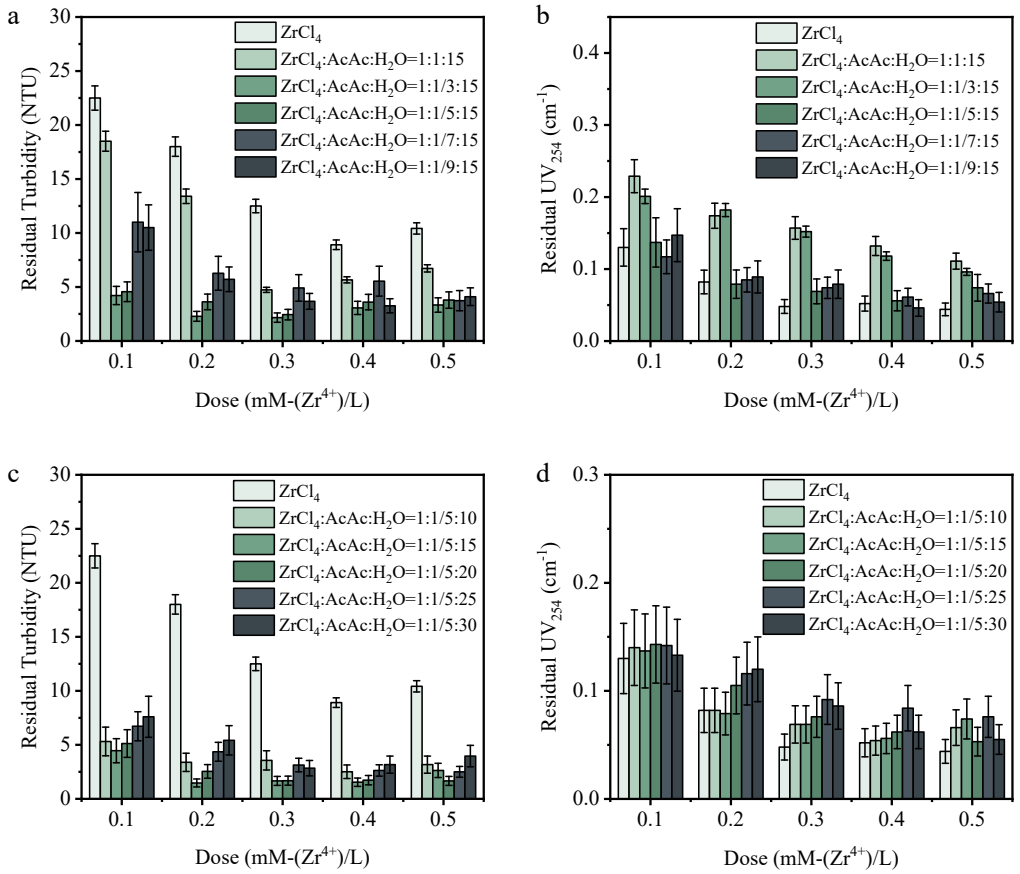

Figure S3. The coagulation performance of ZXC and $ZrCl_4$ in different ratios of precursors; (a, b) $ZrCl_4$:AcAc=1:(1-1/9), (c, d) $ZrCl_4$:H_2O=1:(10-30).

S4. Details of the usability analysis

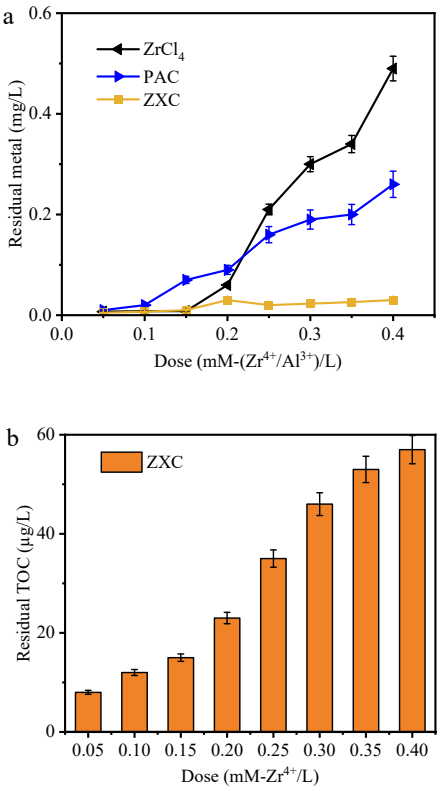

Figure S4. The residual metal of three coagulants (a) and the residual TOC of ZXC (b) after coagulation. Initial pH: 7.

S5 Details about the SEM and mapping of coagulant

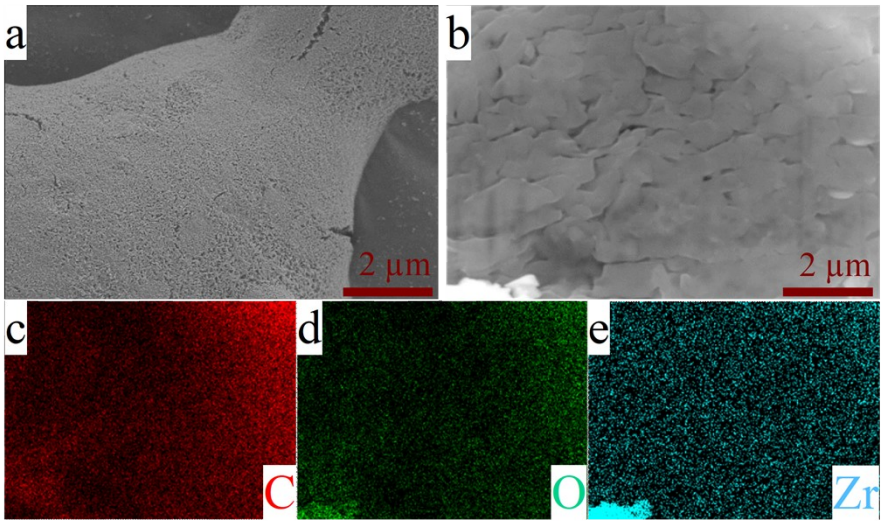

Figure S5. The SEM images of (a) $ZrCl_4$ and (b) ZXC, The mapping images of (c) C, (d) O and (e) Zr for ZXC coagulant.

S6 Details about the XRD spectra of $ZrCl_4$ and ZXC

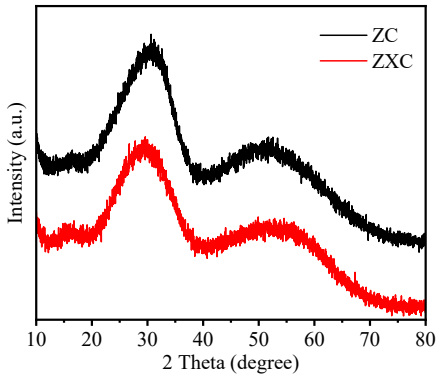

Figure S6. The XRD spectra of Zr hydrolysates from $ZrCl_4$ and ZXC.

S7 Details about the SEM and mapping of floc

The surface characteristics of floc were observed by SEM (**Figure S7**). The surface of ZXC floc was relatively dense and accompanied by a small amount of flake product adhesion (**Figure S7a**). In addition, we observed that the internal structure of the floc seems to be composed of layered clusters, which may be the result of the agglomeration of three-dimensional lamellar products. The three main elements C, O and Zr (**Figure S7b-d**) were evenly distributed in the floc structure.

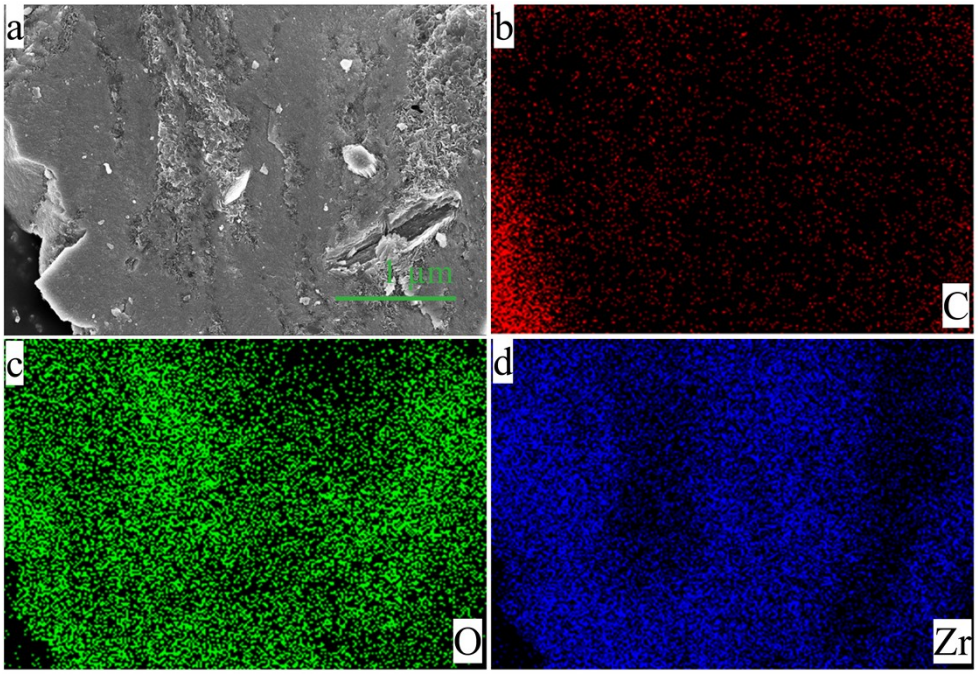

Figure S7. The (a) SEM and mapping images of (b) C, (c) O and (d) Zr for ZXC floc.

S8 Details about the integral area and interval segments

Table S2. The integral area and interval segments of key structures before and after coagulation

pH	Samples	3000-3700 cm^{-1} (-OH)	1500-1800 cm^{-1} (C=O)	1300-1500 cm^{-1} (-COOH)
5	HA	36572	2793	503
	HA- $ZrCl_4$	19370	2120	247
	HA-PAC	17717	2484	367
	HA-ZXC	10756	1122	173
7	HA	14789	1781	846
	HA-$ZrCl_4$	10620	1595	889
	HA-PAC	6567	824	239
	HA-ZXC	11020	730	558
9	HA	4730	763	296
	HA-$ZrCl_4$	9700	1026	305
	HA-PAC	6632	1348	261
	HA-PTC	8904	1046	302

S9. High-resolution XPS C1s spectra at different pH

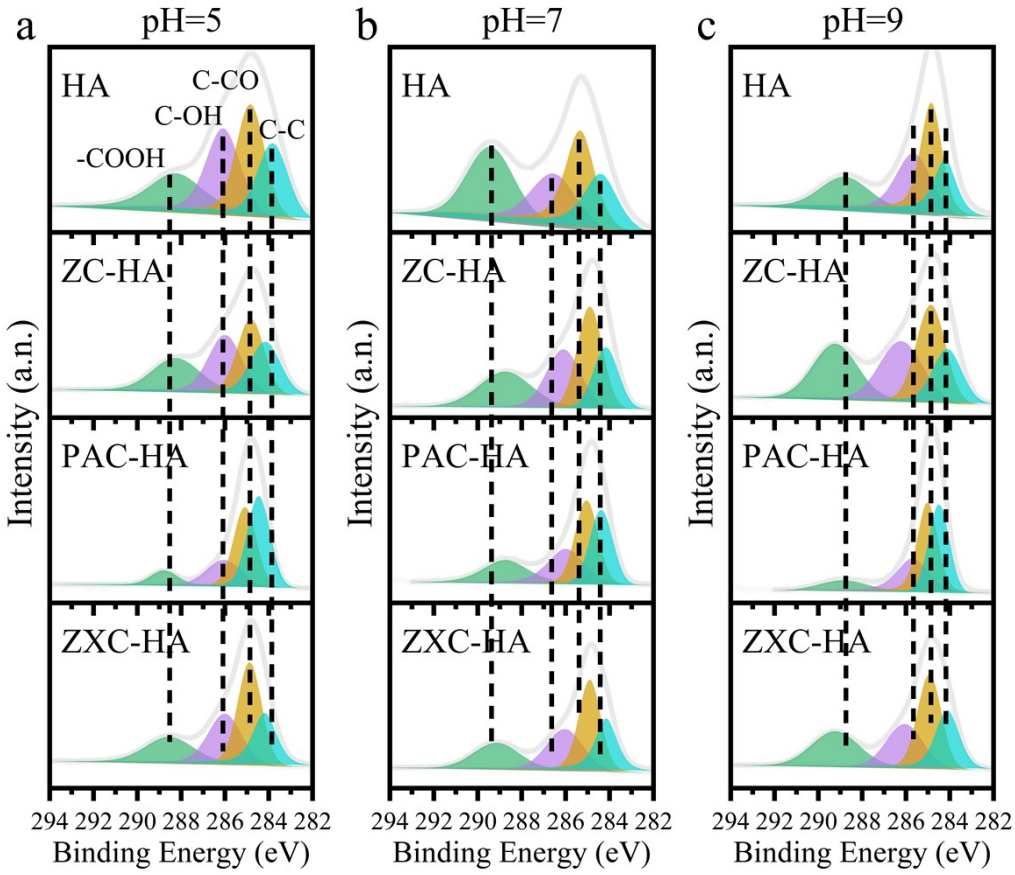

Figure S9. High-resolution C1s XPS spectra of HA and flocs, (a) pH 5, (b) pH 7, (c) pH 9.